ChemComm

COMMUNICATION

View Article Online
View Journal | View Issue

Cite this: *Chem. Commun.*, 2024, **60**, 10330

Received 30th July 2024,
Accepted 21st August 2024

DOI: 10.1039/d4cc03817g

rsc.li/chemcomm

Boosting the photoelectrochemical performance of $BiVO_4$ by borate buffer activation: the role of trace iron impurities†

Xiaohu Cao,[ab] Xuemeng Yu,[c] Xihan Chen *[c] and Ruquan Ye *[ab]

$BiVO_4$ is an attractive photoanode material for water oxidation, but requires surface treatment to improve the energy efficiency and stability. Herein, we investigate the role of borate buffer in activating the $BiVO_4$ photoanode. We found that trace iron impurities in the borate buffer play a critical role in activating the photoanode. By optimizing the activation conditions, the photocurrent density attains 4.5 mA cm^{-2} at 1.23 V_{RHE} without any cocatalysts, alongside a high ABPE value of 1.5% at 0.7 V_{RHE}. Our study discloses the role of iron in the activation effect of borate buffer on the $BiVO_4$ photoanode, which has implications for other catalytic systems.

Bismuth-based materials have extensive applications in various energy catalysis fields, including water splitting and carbon dioxide reduction.[1–8] $BiVO_4$ is regarded as one of the most promising photoanode materials due to its suitable band structure, low cost, and environmental compatibility.[9,10] However, $BiVO_4$ suffers from fast carrier recombination with low carrier mobility and poor surface water oxidation kinetics,[10–12] which makes its photocurrent density far below the theoretical value (~7.5 mA cm^{-2}).[13] Moreover, photostability is also a crucial issue because of the photocorrosion of $BiVO_4$ during photoelectrochemical (PEC) operation.[14] In the last few decades, the surface modification of the $BiVO_4$ photoanode has largely contributed to the advancement of PEC research. The surface modification mostly centers on two strategies. The first strategy is to fabricate a heterogeneous cocatalytic/protective layer.[15,16] The second strategy focuses on the surface treatment of $BiVO_4$, such as creating oxygen vacancies, photoetching, and element doping.[14,17–20]

For the surface treatment of $BiVO_4$, several studies have shown the significant role of buffer solutions. The illumination treatment at open circuit potential has been reported by several works to improve photocurrent performance. This process was regarded as the photocharging effect with the electrolytes of phosphate or borate buffer.[21–24] Recent publications declared that borate electrolytes could modify or photopolarize $BiVO_4$ for better PEC performance.[25–27] The enhancement was attributed to the adsorption of $[B(OH)_4]^-$ species by simple immersion or passivated surface states and oxygen vacancies by photoelectrochemical activation. In addition, the reductive sodium sulfite (Na_2SO_3) was reported to create surface oxygen vacancies and improve photocurrent performance.[19,28] These studies indicate the significance of buffer solution in the surface activation of the $BiVO_4$ photoanode.

Herein, we systematically investigated borate buffer, a popular electrolyte buffer, for its role in the activation of the $BiVO_4$ photoanode. It was found that iron impurities play a critical role in the activation and protection of the $BiVO_4$ photoanode by regulated vanadium dissolution (Fig. 1). The application of appropriate lighting, heating and bias potential will promote this activation performance. After activation by borate buffers, the best photocurrent density reaches 4.5 mA cm^{-2} at 1.23 V_{RHE} without any sacrificial agents or cocatalysts. Meanwhile, the best applied bias photon-to-current efficiency (ABPE) of activated $BiVO_4$ reaches 1.5% at 0.7 V_{RHE}, which is the best ABPE value for bare a $BiVO_4$ photoanode without any cocatalysts. Although iron-mediated surface activation prevents vanadium dissolution to some extent, the long-term stability issue still depends on further employing a vanadium-rich electrolyte,[14] which eventually achieves a highly stable and activated $BiVO_4$ photoanode. These results help to understand the role of iron impurities in buffer solution to the $BiVO_4$ photoanode and help design future practical PEC devices.

To carefully investigate the activation phenomena under various conditions, different treatment processes were applied

[a] *Department of Chemistry, State Key Laboratory of Marine Pollution, City University of Hong Kong, Hong Kong 999077, P. R. China. E-mail: ruquanye@cityu.edu.hk*
[b] *City University of Hong Kong Shenzhen Research Institute, Shenzhen 518057, P. R. China*
[c] *Department of Mechanical and Energy Engineering, Southern University of Science and Technology, Shenzhen, Guangdong, 518055, P. R. China. E-mail: chenxh@sustech.edu.cn*

† Electronic supplementary information (ESI) available. See DOI: https://doi.org/10.1039/d4cc03817g

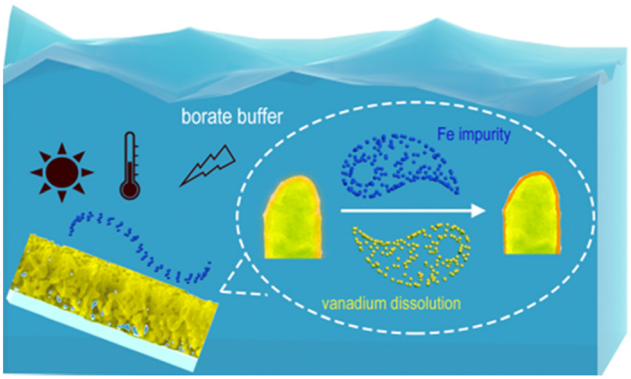

Fig. 1 The borate buffer activation process of the nanoporous $BiVO_4$ photoanode, including the formation of an Fe active layer and the dissolution of vanadium species.

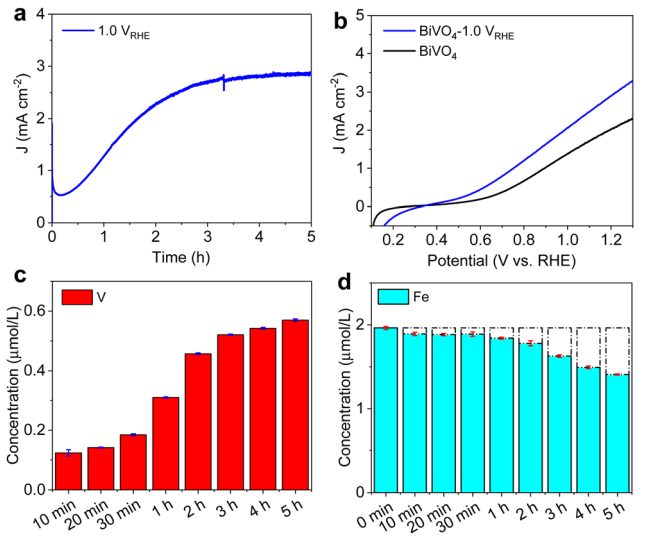

Fig. 2 (a) J–t curve at 0.6 V *vs.* RHE of $BiVO_4$ photoanodes tested in 1 M KBi pH 9.3 under AM 1.5 G irradiation (100 mW cm^{-2}). (b) The LSV curves before and after the J–t curve. ICP results of (c) V and (d) Fe in electrolyte used in the J–t curve during different times.

to $BiVO_4$ photoanodes with 1 M KBi pH 9.3 borate buffer, including lighting, heating, and bias potential (Fig. S1, ESI†). The activated $BiVO_4$ photoanodes discussed above achieve an impressive improvement in photocurrent density and onset potential through different treatment processes. Different activation mechanisms have been proposed, including the passivation of the surface states, the adsorption of anionic species, the generation of oxygen vacancies, and the formation of a homologous heterojunction.[22,24,26,27,29] These mechanisms might contribute to the enhanced activity but remain unconsolidated.

In our discussion, external stimulations of illumination and bias potential were applied to investigate the activation effect of borate buffer on the $BiVO_4$ photoanode. By comparing the activation performance at different concentrations (Fig. S2 and S3, ESI†), it clearly demonstrates that the best borate concentration of activation condition is in the range of 0.5–2 M (1 M used in this work). The investigation results also suggest that the alkali metal cations are not the key factor of the activation phenomenon (Fig. S4, ESI†). Moreover, the other anion electrolyte treatments have no obvious photocurrent improvement to $BiVO_4$ photoanodes compared with borate buffer (Fig. S5 and S6, ESI†). These results suggest that anion species can potentially impact the activation performance of the $BiVO_4$ material, particularly its chemical stability related to vanadium dissolution.[30] The activation performance of $BiVO_4$ photoanodes was investigated in different pH values (Fig. S7–S9, ESI†). The results demonstrate that medium alkaline (pH 9.3) borate buffer has a better activation performance than those of neutral (pH 7) and strong alkaline (pH 12) buffers.

In order to monitor the activation mechanism accurately, chronoamperometry under illumination was used to investigate the activation effect for $BiVO_4$ photoanodes. Fig. 2 shows that under 0.6 V_{RHE} illumination, the photocurrent decreases rapidly in the first 10 min, then increases to a maximum plateau after about 4 hours, resulting in a photocurrent improvement to 4.5 mA cm^{-2} at 1.23 V_{RHE}. Fig. 2c and d monitor the concentration changes of elements V and Fe by inductively coupled plasma (ICP) analysis of borate electrolyte during the J–t tests. In the first 10 min, the dissolved V from the $BiVO_4$ electrode reaches around 0.05 μM, further increasing until the photocurrent nears the plateau. As the crucial part of the activation effect, Fig. 2d reveals the most critical role of the Fe impurity in the borate electrolyte. The initial concentration of impurity Fe is about 2 μM in 1 M borate buffer. The Fe concentration in electrolytes decreases with increasing photocurrent density in the J–t curve. Around the photocurrent plateau, both the rates of V dissolution and Fe reduction in the borate electrolyte become smaller. The $BiVO_4$ photoanode at 1.0 V_{RHE} demonstrates the same tendency of V and Fe elements during activation treatment in the borate electrolyte (Fig. S10 and S11, ESI†). It is apparent that bias potential will also impact the activation performance of the $BiVO_4$ photoanode (Fig. S12, ESI†). The ICP results of the remaining electrolytes demonstrate that the bias potential remarkably influences vanadium dissolution, while the variation in Fe content is negligible. Meanwhile, a smaller bias potential at 0.4 V_{RHE} was applied to the $BiVO_4$ photoanode for J–t tests (Fig. S13, ESI†). The activation takes more time to reach the plateau because 0.4 V_{RHE} bias is close to the flat band potential of $BiVO_4$.

X-ray photoelectron spectroscopy (XPS) was performed on bare $BiVO_4$ and activated $BiVO_4$ to further probe the surface species. As shown in Fig. 3a, the activated $BiVO_4$ photoanode exhibits the typical Fe 2p characteristic peak, while the bare $BiVO_4$ photoanode shows no Fe signal. The spectra of Bi 4f and V 2p peaks display negligible shifts before and after activation (Fig. S14, ESI†). However, the photoelectrochemical activation of the $BiVO_4$ photoanode experiences a strong signal decrease for Bi 4f and V 2p peaks. Table S1 (ESI†) summarizes the atomic ratio of surface elements from XPS spectra. The surface elemental composition shows a considerable decrease for Bi and V, especially. This results from the formation of the surface Fe

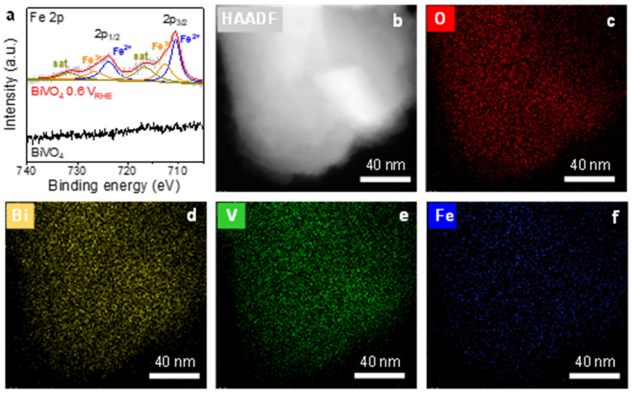

Fig. 3 (a) Fe 2p XPS spectrum of $BiVO_4$ and activated $BiVO_4$, (b) TEM and (c)–(f) TEM-EDS elemental mapping images of activated $BiVO_4$.

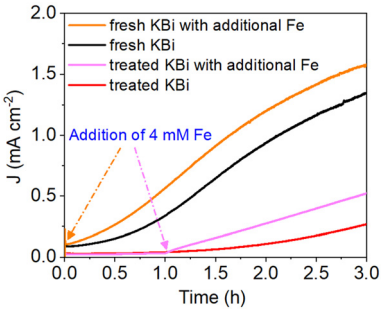

Fig. 4 *J*–*t* curve at 0.6 V *vs.* RHE of $BiVO_4$ photoanodes tested in KBi buffer with/without purification treatment for removal of Fe impurities. Change of photocurrent upon an intentional addition of 4 μM Fe^{2+} at 1 hour during the *J*–*t* test.

active layer and the vanadium dissolution, as discussed above.[19,31] In addition, the previous works reported that the B 1s spectrum after treatment shows a weak peak due to boron oxide formation.[24,27,32] However, the B 1s spectrum exhibits no distinct characteristic peaks, although we have enhanced the number of XPS scans. Thus, it is speculated that the performance improvement is from forming the Fe active layer on the $BiVO_4$ photoanode. Furthermore, transmission electron microscope (TEM) images reveal the irregular nanorod structure of the $BiVO_4$ photoanode material (Fig. S15, ESI†). This indicates that borate activation produces an ultrathin Fe active layer on the surface of $BiVO_4$. The TEM elemental mapping images of activated $BiVO_4$ display that Bi and V elements are mainly dispersed in the core region of the nanorod (Fig. 3a). Meanwhile, as expected, the Fe element distributes randomly on the surface of the $BiVO_4$ nanorods, which comes from the Fe impurity in the borate buffer as discussed above.

The iron impurities have been demonstrated to be unavoidable for KBi buffer, which generally originates from the chemical reagents themselves.[33,34] Meanwhile, Fe species, including Fe oxides, Fe oxyhydroxides, and Fe borates, have usually been reported as one of the most effective cocatalysts for $BiVO_4$ photoanodes.[31,35,36] Here, we remove most of the Fe impurities in the KBi buffer by a two-step electrolysis using Ti foil electrodes. The electrolyte purification results were evaluated by ICP tests (Fig. S16, ESI†). More than half of the Fe impurities were removed after two-step electrolytic purification. As shown in Fig. 4, since there are still Fe impurities that cannot be completely removed from the treated KBi buffer, the photocurrent of the $BiVO_4$ photoelectrode rises more slowly than that in the fresh KBi buffer. To further verify the critical role of iron impurities on photocurrent rise, 4 μM of Fe source was intentionally added during the *J*–*t* test. It was observed that the addition of Fe source led to a rapid increase in the photocurrent. The results verify that the activation performance comes from the formation of an Fe active layer. When the test time is extended (Fig. S17, ESI†), the photocurrent in the treated KBi buffer can still reach about 1.9 mA cm^{-2}, albeit taking more time. Nevertheless, both fresh and treated KBi buffer cannot substantially prevent the occurrence of photocorrosion caused by vanadium dissolution. Once the balance between the formation of the Fe active layer and the vanadium dissolution is reached, which is shown as the photocurrent plateau in the *J*–*t* curves, the photocurrent of the photoelectrode starts to decrease. This decrease is primarily due to the loss of V^{5+} ions in the $BiVO_4$ lattice, which causes photocorrosion.[14] This issue is also proved by one piece of $BiVO_4$ electrode activated at *J*–*t* cycles replacing with a new electrolyte each time (Fig. S18 and S19, ESI†). For long-term stability, excessive vanadium was added to the KBi buffer to inhibit photocorrosion caused by vanadium dissolution according to Le Chatelier's principle (Fig. S20, ESI†). This helps obtain stable photocurrent properties of composite $BiVO_4$ photoanodes after self-activation by iron impurities.

The surface Fe active layer greatly improves the performance of the $BiVO_4$ photoanode. The electrochemical active surface area has almost tripled compared to the bare $BiVO_4$ photoanode (Fig. S22, ESI†). This indicates that the Fe active layer can increase the surface active sites of $BiVO_4$ and improve the PEC performance. Both $BiVO_4$ and activated $BiVO_4$ photoanodes have almost identical LSV curves with the addition of $NaSO_3$, indicating that their $\eta_{separation}$ values are very close (Fig. S23, ESI†). The activated $BiVO_4$ photoanode shows a charge injection efficiency of 88%, which is about twice as high as the $\eta_{injection}$ of bare $BiVO_4$ at the same bias potential, leading to better surface water oxidation efficiency.[22] The open circuit potential (OCP) tests were applied to explore the merit of the Fe active layer to the $BiVO_4$ photoanode (Fig. S24, ESI†). It is vivid in demonstrating the suppression of η_H and the enhancement of V_{ph} resulting from the elimination of surface states. Then, the activated $BiVO_4$ photoanode obtains attractive onset potential and water oxidation photocurrent. Transient absorption spectroscopy (TAS) was employed to investigate the behavior of charge carriers in both bare and activated $BiVO_4$ samples (Fig. S25–S27, ESI†). Activated $BiVO_4$ displays a slower rate of carrier recombination, which is attributed to its longer carrier lifetime. This observation suggests that the Fe active layer facilitates the transfer of holes to the solution, leading to more efficient inhibition of electron–hole recombination. Fig. 5a displays that the activation performance by the Fe impurities is among the best performances of the $BiVO_4$ photoanode

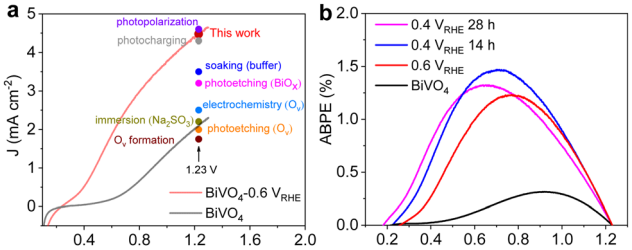

Fig. 5 (a) LSVs of the $BiVO_4$ photoanode for the best activation photocurrent in this work, which is also compared with the results of other unmodified $BiVO_4$ photoanodes. (b) ABPEs calculated by LSV curves.

without extra cocatalysts (details in Table S3, ESI†). Furthermore, ABPEs in Fig. 5b were calculated according to the corresponding LSV curves (Fig. S12 and S13, ESI†). The ABPE value of bare $BiVO_4$ is only 0.3%, which is greatly improved after forming the Fe active layer. The best ABPE value of activated $BiVO_4$ is 1.5% at 0.7 V_{RHE}.

In summary, we carefully investigate how trace iron impurities in borate buffer affect the $BiVO_4$ photoanode activation. Using a vanadium-rich solution and iron-activated photoanode, we achieve long-term stability at a photocurrent density of 4.5 mA cm^{-2} at 1.23 V_{RHE} without any cocatalysts and an attractive ABPE value of 1.5% at 0.7 V_{RHE}. The discovery and discussion of trace iron impurities in borate buffer sheds light on the significant activation effect of the $BiVO_4$ photoanode and may inspire promising applications in other catalytic reactions. Future investigation of the chemical status and activation mechanisms of iron can help the rational design of effective catalysts.

Ruquan Ye acknowledges support from Guangdong Basic and Applied Basic Research Fund (2022A1515011333, 2024A1515030164), Hong Kong Research Grant Council (11309723, 11310624), the Shenzhen Science and Technology Program (JCYJ20220818101204009), State Key Laboratory of Marine Pollution (SKLMP/SCRF/0060) and CityU Applied Research Grant (9667254). Xihan Chen acknowledges the support from the National Natural Science Foundation of China (22373046).

Data availability

The data supporting this article have been included as part of the ESI.†

Conflicts of interest

There are no conflicts to declare.

Notes and references

1 S. Khatun and P. Roy, *Chem. Commun.*, 2020, **56**, 7293–7296.
2 M. Miola, B. C. A. de Jong and P. P. Pescarmona, *Chem. Commun.*, 2020, **56**, 14992–14995.
3 Y. Wang, Z. Huang, Y. Lei, J. Wu, Y. Bai, X. Zhao, M. Liu, L. Zhan, S. Tang, X. Zhang, F. Luo and X. Xiong, *Chem. Commun.*, 2022, **58**, 3621–3624.
4 Y. Hu, J. Liang, Y. Gu, S. Yang, W. Zhang, Z. Tie, J. Ma and Z. Jin, *Nano Lett.*, 2023, **23**, 10512–10521.
5 L. Wang, Y. Zhang, W. Li and L. Wang, *Mater. Rep.: Energy*, 2023, **3**, 100232.
6 M. Wang, H. Wang, Y. Gu, M. Zhu, M. Kumar, J. Liang, Z. Tie, J. Ma and Z. Jin, *ACS Mater. Lett.*, 2023, **6**, 100–108.
7 S. Yang, M. Jiang, W. Zhang, Y. Hu, J. Liang, Y. Wang, Z. Tie and Z. Jin, *Adv. Funct. Mater.*, 2023, **33**, 2301984.
8 X. Tao, X. Zhou and R. Li, *Chem. Commun.*, 2024, **60**, 5136–5148.
9 C. Jiang, S. J. A. Moniz, A. Wang, T. Zhang and J. Tang, *Chem. Soc. Rev.*, 2017, **46**, 4645–4660.
10 H. L. Tan, R. Amal and Y. H. Ng, *J. Mater. Chem. A*, 2017, **5**, 16498–16521.
11 F. F. Abdi, T. J. Savenije, M. M. May, B. Dam and R. van de Krol, *J. Phys. Chem. Lett.*, 2013, **4**, 2752–2757.
12 M. Li, Y. Deng, G. Wu, S. Xue, Y. Yan, Z. Liu, J. Zou, D. Yang and A. Dong, *Aggregate*, 2021, **2**, e17.
13 C. Liu, N. P. Dasgupta and P. Yang, *Chem. Mater.*, 2014, **26**, 415–422.
14 D. K. Lee and K.-S. Choi, *Nat. Energy*, 2018, **3**, 53–60.
15 D. Lee, A. Kvit and K.-S. Choi, *Chem. Mater.*, 2018, **30**, 4704–4712.
16 Y. Shi, Y. Yu, Y. Liang, Y. Du and B. Zhang, *Angew. Chem., Int. Ed.*, 2019, **58**, 3769–3773.
17 S. Wang, T. He, P. Chen, A. Du, K. K. Ostrikov, W. Huang and L. Wang, *Adv. Mater.*, 2020, **32**, e2001385.
18 S. Wang, P. Chen, J. H. Yun, Y. Hu and L. Wang, *Angew. Chem., Int. Ed.*, 2017, **56**, 8500–8504.
19 S. Feng, T. Wang, B. Liu, C. Hu, L. Li, Z. J. Zhao and J. Gong, *Angew. Chem., Int. Ed.*, 2020, **59**, 2044–2048.
20 A. J. Rettie, H. C. Lee, L. G. Marshall, J. F. Lin, C. Capan, J. Lindemuth, J. S. McCloy, J. Zhou, A. J. Bard and C. B. Mullins, *J. Am. Chem. Soc.*, 2013, **135**, 11389–11396.
21 B. J. Trześniewski and W. A. Smith, *J. Mater. Chem. A*, 2016, **4**, 2919–2926.
22 B. J. Trześniewski, I. A. Digdaya, T. Nagaki, S. Ravishankar, I. Herraiz-Cardona, D. A. Vermaas, A. Longo, S. Gimenez and W. A. Smith, *Energy Environ. Sci.*, 2017, **10**, 1517–1529.
23 E. Y. Liu, J. E. Thorne, Y. He and D. Wang, *ACS Appl. Mater. Interfaces*, 2017, **9**, 22083–22087.
24 N. J. Firet, A. Venugopal, M. A. Blommaert, C. Cavallari, C. J. Sahle, A. Longo and W. A. Smith, *Chem. Mater.*, 2019, **31**, 7453–7462.
25 Z. Kang, X. Lv, Z. Sun, S. Wang, Y.-Z. Zheng and X. Tao, *Chem. Eng. J.*, 2021, **421**, 129819.
26 R. T. Gao and L. Wang, *Angew. Chem., Int. Ed.*, 2020, **59**, 23094–23099.
27 Q. Meng, B. Zhang, L. Fan, H. Liu, M. Valvo, K. Edstrom, M. Cuartero, R. de Marco, G. A. Crespo and L. Sun, *Angew. Chem., Int. Ed.*, 2019, **58**, 19027–19033.
28 Y. Peng, H. Wu, M. Yuan, F.-F. Li, X. Zou, Y. H. Ng and H.-Y. Hsu, *Sustainable Energy Fuels*, 2021, **5**, 2284–2293.
29 X. Chen, C. Zhen, N. Li, N. Jia, X. Xu, L. Wang and G. Liu, *Small Methods*, 2023, **7**, e2201611.
30 F. M. Toma, J. K. Cooper, V. Kunzelmann, M. T. McDowell, J. Yu, D. M. Larson, N. J. Borys, C. Abelyan, J. W. Beeman, K. M. Yu, J. Yang, L. Chen, M. R. Shaner, J. Spurgeon, F. A. Houle, K. A. Persson and I. D. Sharp, *Nat. Commun.*, 2016, **7**, 12012.
31 H. Xu, W. Fan, Y. Zhao, B. Chen, Y. Gao, X. Chen, D. Xu and W. Shi, *Chem. Eng. J.*, 2021, **411**, 128480.
32 M. Wang, H. Zheng, Q. Liu, C. Niu, Y. Che and M. Dang, *Spectrochim. Acta, Part A*, 2013, **114**, 74–79.
33 Y. Kuang, Q. Jia, G. Ma, T. Hisatomi, T. Minegishi, H. Nishiyama, M. Nakabayashi, N. Shibata, T. Yamada, A. Kudo and K. Domen, *Nat. Energy*, 2016, **2**, 16191.
34 A. M. Smith, L. Trotochaud, M. S. Burke and S. W. Boettcher, *Chem. Commun.*, 2015, **51**, 5261–5263.
35 S. Wang, P. Chen, Y. Bai, J. H. Yun, G. Liu and L. Wang, *Adv. Mater.*, 2018, **30**, e1800486.
36 M. N. Shaddad, M. A. Ghanem, A. M. Al-Mayouf, S. Gimenez, J. Bisquert and I. Herraiz-Cardona, *ChemSusChem*, 2016, **9**, 2779–2783.